Simulation and analysis of ZnO/SWCNT solar cell using the SCAPS-1D program

Abdelhafid Najim[1*], *Abdelmounaim* Laassouli[1], *Lhouceine* Moulaoui[2], *Omar* Bajjou[1], and *Khalid* Rahmani[3]

[1]Laboratory of Engineering in Chemistry and Physics of Matter (LIPCM), Faculty of Sciences and Technics, Sultan Moulay Slimane University, B.P 523, 23000 Beni Mellal, Morocco
[2]Research Laboratory in Physics and Sciences for Engineers (LRPSI), Poly-disciplinary Faculty, Sultan Moulay Slimane University, Beni Mellal-Morocco
[3]PSES, ERC, Ecole Normale Supérieur, Mohammed V University in Rabat, P. O. Box: BP5118 Takkadoum Rabat-10000, Morocco

Abstract. The exceptional optical and electrical properties of Single-Walled Carbon Nanotube (SWCNT) material present significant potential for solar cells, especially when used with zinc oxide (ZnO) as a buffer layer. This study examines the electrical characteristics and performance metrics of ZnO/SWCNT solar cells using the SCAPS-1D software. Understanding the impact of various factors such as temperature, thickness, and operational resistors (R_s and R_{sh}) on the performance of this photovoltaic device is crucial. The ZnO/SWCNT solar cell demonstrates impressive power conversion efficiency ($\eta = 24.42$ %), an open-circuit voltage (V_{oc}) of 0.7740 V, a short-circuit current density (J_{sc}) of 40.303777 mA/cm², and a fill factor (FF) of 78.27 %. These parameters can be further enhanced through optimization, resulting in an efficiency of $\eta = 26.44$ %. Therefore, the results of this simulation suggest the potential for highly efficient solar cells and significant future technological advancements.

Keywords: SCAPS-1D, ZnO, SWCNT, solar cell, photovoltaic parameters.

1 Introduction

Solar energy is gaining popularity because it is clean, affordable, and renewable, which highlights the importance of utilizing this abundant resource. However, a significant challenge in effectively harnessing solar energy is the lack of suitable solar equipment with high power conversion efficiency, which is essential for converting solar energy into usable forms [1]. A major focus of current research is the development of highly efficient solar cells. These solar photovoltaic cells capture sunlight and convert it into electricity. The materials used to produce crystalline and non-crystalline photovoltaic cells include both elemental and composite substances. Despite the diversity of industries and technologies in the market, over 85 % of solar cells are silicon-based. This predominance is largely driven by the expansion of the silicon-intensive nanoelectronics industry and the superior quality of silicon cells [2].

* Corresponding author: abdelhafid.najim@usms.ma

In this context, ZnO is a suitable material for use as an electron transport layer (ETL) in solar cells because of its wide bandgap (~3.2 eV), excellent transparency, high electron mobility, high electron affinity, and appropriate work function (~4.3 eV) [3].

Graphene, a semimetal with a zero band gap at the Dirac point, belongs to the family of 2D materials and has garnered significant interest across various fields due to its extraordinary physical properties [4]. The carbon atoms in graphene possess four valence electrons ($2s^2\ 2p^2$) [5]. Within the graphene plane, the 2s, $2p_x$, and $2p_y$ orbitals of each carbon atom undergo hybridization to form three sp^2 hybrid orbitals [6]. The $2p_z$ orbital remains unhybridized and perpendicular to the plane of the graphene layer. These hybrid orbitals (2s, $2p_x$, and $2p_y$) form σ bonds between adjacent carbon atoms within the plane, while the unhybridized $2p_z$ orbital contributes to π bonds normal to the graphene plane [7]. Graphene can be seen as the foundational unit of three carbon allotropes—graphite, buckyballs, and carbon nanotubes (CNTs)—that are formed by rolling or folding graphene into various structures [8]. In recent years, carbon nanotubes have been thoroughly researched due to their critical role in nanotechnology [9]. Previous studies indicate that combining CNTs with metal electrodes results in better performance compared to using CNTs alone as both electrodes and hole transport layers. CNTs offer various potential applications in perovskite solar cells [10,12], including transparent conductive electrodes, materials for hole and electron transport, interlayers, and back electrodes [13]. This paper utilizes SCAPS 1D software to simulate and optimize the layers of a planar structure involving ZnO and CNTs. It represents a distinctive effort in optimizing the photovoltaic parameters of each layer in ZnO/CNT solar cell to achieve peak efficiency [14].

Our paper is organized as follows: Section 2 details the computational methods employed, specifically the use of SCAPS-1D in solar cell simulations. Section 3 discusses the numerical results obtained. The study concludes with Section 4.

Indications of nomenclature	
SWCNT : Single-Walled Carbon Nanotube ZnO : Zinc oxide SCAPS-1D : One dimensional solar cell capacitance simulator T : Temperature d : Thickness N_A : Shallow uniform acceptor density N_D : Shallow uniform donor density R_s : Series resistance R_{sh} : Shunt resistance J_n : Electron current density. J_p : Hole current density. R : Rate of electron hole pairs recombination. G : Rate of electron hole pairs generation. D_p : Diffusion coefficient for holes. D_n : Diffusion coefficient for electrons. n : Concentration of free carrier electrons. p : Concentration of free carrier holes. φ : Metal work function	S_h : Surface recombination velocity for holes S_e : Surface recombination velocity for electrons n : So-called ideality factor. q : Elementary charge. K_B : Boltzmann constant. I_{max} : Photocurrent for maximum power output. V_{max} : Photovoltage for maximum power output. J_{sc} : Short-circuit photocurrent. P_{in} : Incident power. V : Applied voltage. J_0 : Saturation current. J_L : Photogenerated current. E_g : Band gap χ : Electron affinity ε_r : Dielectric permittivity (relative) N_c : CB effective density of states N_v : VB effective density of states V_e : Electron thermal velocity V_h : Hole thermal velocity μ_n : Electron mobility μ_p : Hole mobility

2 Materials and methodology

2.1 Numerical simulation using SCAPS-1D

Numerical design and modeling of solar cells are essential tools in photovoltaic research. These computational methods offer a prototype to comprehend the functioning and forecast the physical behavior of devices based on several critical parameters. These parameters, which significantly affect the performance of solar cells, include film thickness, band gap, electron affinity, carrier concentration, defect density, work function, shunt and series resistances, and operating temperature [15]. Several packages have been developed and made freely available, such as SCAPS-1D, which have played a significant role in advancing solar cell research [16]. SCAPS-1D is one of the most extensively used simulators for perovskite-based solar cells, developed at the University of Gent [17]. This simulation program numerically solves fundamental one-dimensional semiconductor equations under steady-state conditions [18]. The simulation software solves fundamental semiconductor physics equations, including the continuity equations for both electrons and holes, and the Poisson equation, which relates charge to the electrostatic potential [19]. The core concept behind this application is to use various iterative techniques to solve continuity problems alongside Poisson equations. Mathematically, these equations can be expressed as [20,21]:

$$\nabla^2\psi = \frac{q}{\varepsilon}(n - p + N_A - N_D + \rho(n,p)) \tag{1}$$

Where,
ψ : is the electrostatic potential.
$\rho(n,p)$: is the charge located in deep states.

$$\frac{\partial n}{\partial t} = \frac{1}{q}\nabla.J_n + G - R \tag{2}$$

$$\frac{\partial p}{\partial t} = -\frac{1}{q}\nabla.J_P + G - R \tag{3}$$

$$J_n = qn\mu_n E + qD_n\nabla_n \tag{4}$$

$$J_p = qp\mu_p E - qD_p\nabla_p \tag{5}$$

The performance parameters of a solar cell average J_{sc}, V_{oc}, FF, and η are determined using the following equation [22]:

$$V_{oc} = \frac{nK_BT}{q}\ln\left[\frac{J_{sc}}{J_0} + 1\right] \tag{6}$$

$$FF = \frac{I_{max}.V_{max}}{J_{sc}.V_{oc}} \tag{7}$$

$$\eta = \frac{J_{sc}.V_{oc}.FF}{P_{in}} \tag{8}$$

$$J = J_0\left[exp\left(\frac{qV}{nK_BT}\right) - 1\right] - J_L \tag{9}$$

where,
$\frac{nKT}{q}$: is the thermal voltage.

2.2 Device structure and simulation parameters

In this work, simulations using the SCAPS-1D software employ a cell model with the configuration FTO/n-ZnO/p-SWCNT under an incident solar power of 1000 W/m². The cell is exposed to simulated light at a temperature of 300 K. This structure comprises FTO as the window layer, a ZnO layer as n-type semiconductors, and SWCNT layers as p-type semiconductors. Fig. 1 depicts the layered structure of the ZnO/SWCNT solar cell. Illumination occurs through the FTO. The light passes through the electron transport layer (ZnO), acting as a buffer layer, and then enters the absorber layer (SWCNT), leading to the hole transport material. The schematic of the FTO/ZnO/SWCNT cell is shown in Fig. 1. The parameters used for simulating this solar cell are detailed in Tables 1 and 2.

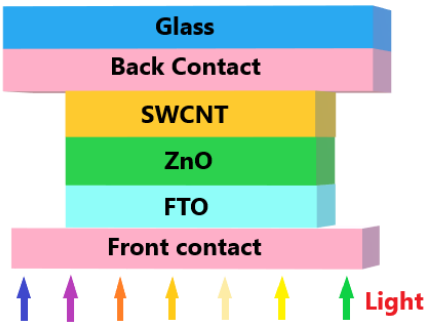

Fig. 1. Schematic of the photovoltaic device structure of ZnO/SWCNT solar cell.

Table. 1. A summary of standard cell parameters used in simulation of ZnO/SWCNT [23–25].

Parameter	FTO	n-ZnO	p-SWCNT
d (μm)	0.5	0.05	0.6
E_g (eV)	3.5	3.3	1.55
χ (eV)	4	4	3.64
εr	9	9	9
N_c (1/cm^3)	2.2 x 10^{18}	3.7 x 10^{18}	2.2 x 10^{18}
N_v (1/cm^3)	1.8 x 10^{19}	1.8 x 10^{19}	1.8 x 10^{19}
V_e (cm/s)	10^7	107	10^7
V_h (cm/s)	10^7	107	10^7
μ_n (cm²/Vs)	20	100	100
μ_p (cm²/Vs)	10	25	38.69
N_D (1/cm^3)	2 x 10^{19}	10^{18}	0
N_A (1/cm^3)	0	0	4 x 10^{18}

Table 2. Contacts electrical properties used in the SCAPS-1D simulation.

Parameter	Back contact	Front contact
φ (eV)	4.7	4.26
S_e (cm/s)	10^5	10^7
S_h (cm/s)	10^7	10^5

3 Results and discussions

3.1 Current-voltage characteristics (J–V)

Fig. 2 presents the J-V characteristics of the ZnO/SWCNT solar cell, showing an open circuit voltage of 0.7740 V, a short circuit current density of 40.303777 mA/cm², a fill factor of 78.27 %, and an efficiency of 24.42 %. These metrics indicate a high-quality junction with efficient charge carrier production. The diode-like curve shape reveals substantial current generation at low voltages. A high FF points to minimal series and parallel resistance losses. In summary, the J-V characteristics confirm the solar cell's effectiveness in converting sunlight into electricity, making the ZnO/SWCNT cell a strong candidate for efficient solar energy conversion.

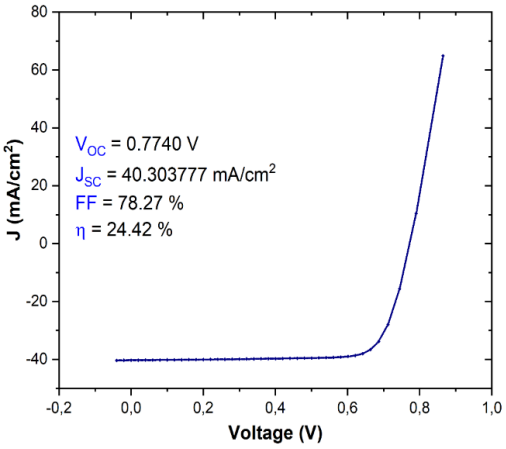

Fig. 2. J–V characteristic curves of the ZnO/SWCNT solar cell as a function of temperature.

3.2 Temperature effect

In this section, we examined how temperature affects the performance of the ZnO/SWCNT solar cell. We varied this temperature from 300 K to 500 K. Fig. 3 illustrates the effect of temperature on the photovoltaic parameters of the ZnO/SWCNT solar cell. According to Fig. 3(a), the V_{oc} decreases as temperature increases, from about 0.774 V to 0.4899 V between 300 K and 500 K. Conversely, the J_{sc} rises slightly with temperature, increasing from approximately 40.30378 mA/cm² to 40.33714 mA/cm² between 300 K and 400 K, then decreasing to 40.32704 mA/cm² at 500 K. Fig. 3(b) shows a reduction in FF and efficiency as temperature rises. The FF declines from approximately 78.27% to 64.2%, while efficiency drops from 24.42% to 12.68%. These findings indicate that higher temperatures negatively affect the FF and η parameters. The reduction in V_{oc} is due to increased thermal recombinations, while the increase in J_{sc} is likely due to improved charge carrier generation at temperatures below 400 K. However, the overall degradation of FF and η suggests that recombination and series resistance losses increase with temperature, thereby reducing the solar cell's overall efficiency. Finally, at higher temperatures, increased thermal agitation leads to greater electron-hole recombination, reducing the number of charge carriers available for the photo-generated current and lowering V_{oc}. This, combined with rising series resistance (from phonon scattering) and reduced shunt resistance (from leakage currents), decreases the FF, impairing the cell's power conversion efficiency. While the J_{sc} may slightly

increase due to improved carrier generation, the overall efficiency drops as V_{oc} and FF decline.

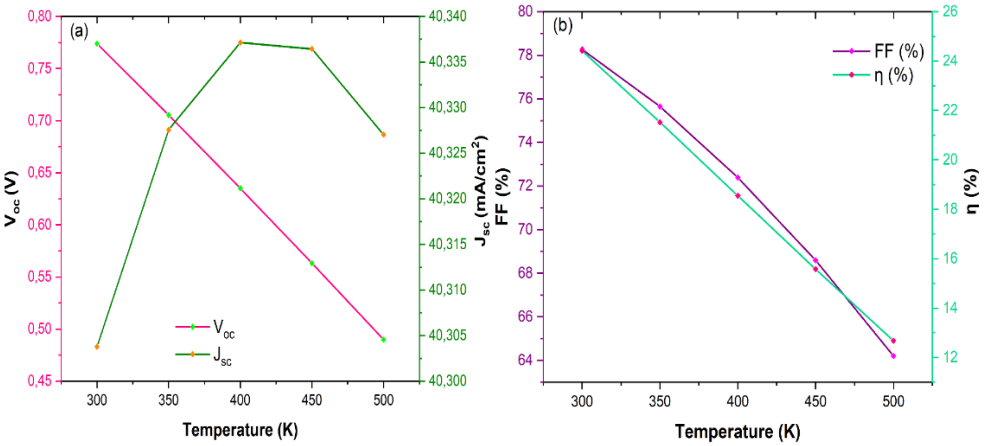

Fig. 3. Performance parameters of the ZnO/SWCNT solar cell as a function of temperature.

3.3 Influence of the SWCNT Layer Thickness

To evaluate the impact of the SWCNT layer thickness, we performed simulations using the SCAPS-1D software, varying the thickness from 0.5 µm to 3 µm. Fig. 4 demonstrates the effect of SWCNT layer thickness on the photovoltaic parameters of the ZnO/SWCNT solar cell. The V_{oc} increases from 0.774 V to 0.7786 V as the SWCNT layer thickness grows from 0.5 µm to 3 µm, indicating that thicker SWCNT layers enhance charge separation and reduce nonradiative recombination, resulting in higher voltage. The J_{sc} also rises, from 40.30378 mA/cm² to 43.3458 mA/cm², due to the increased light absorption with thicker layers, which generates more electron-hole pairs and boosts the current produced by the solar cell. The FF fluctuates slightly between 78.27 % and 78.35 %, indicating that the SWCNT layer thickness does not significantly affect the resistive losses of the ZnO/SWCNT solar cell. Additionally, the efficiency improves from 24.42 % to 26.44 % as the SWCNT layer thickness increases, attributed to the enhanced absorption of incident photons with thicker SWCNT layers.

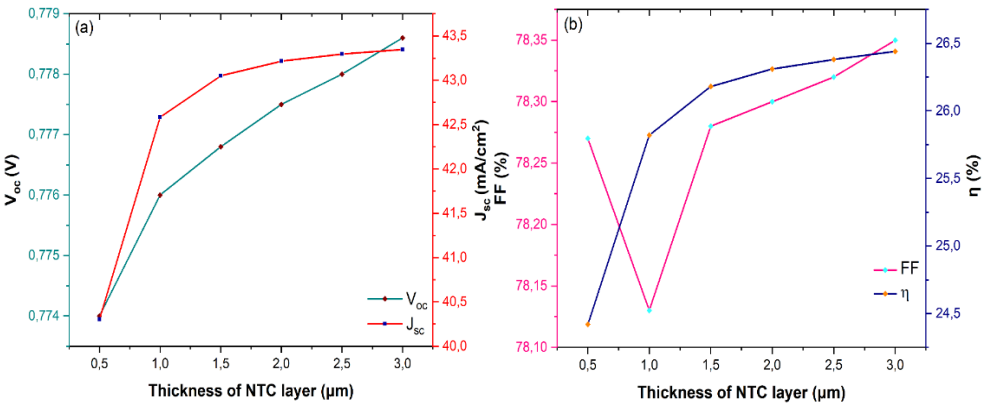

Fig. 4. Effect of thickness of SWCNT layer on the performance parameters of the ZnO/SWCNT solar cell.

3.4 Influence of the ZnO layer thickness

Fig. 5 illustrates the impact of the ZnO layer thickness on the photovoltaic parameters of the ZnO/SWCNT solar cell, with the thickness varying from 0.5 µm to 3 µm. The V_{oc} remains constant at 0.774 V as the ZnO layer thickness increases from 0.5 µm to 3 µm, indicating that changes in the ZnO layer thickness do not significantly affect the internal electric field responsible for charge separation and the open-circuit voltage. The J_{sc} decreases from 40.30378 mA/cm² to 40.25637 mA/cm², then remains nearly constant. This slight reduction may occur because a thicker ZnO layer can increase the recombination of electron-hole pairs before they are collected, reducing the short-circuit current slightly. The FF decreases from 78.27 % to 77.89 %, likely due to increased resistive losses in the solar cell as the ZnO layer thickness increases. Greater thickness can lead to higher series resistance, impacting the FF. Additionally, the efficiency decreases from 24.42 % to 24.27 % as the ZnO layer thickness increases. This reduction in efficiency is primarily due to the decreases in J_{sc} and FF. Although these reductions are small, they still affect the overall performance of the solar cell, reducing its efficiency. In summary, increasing the ZnO layer thickness beyond a certain point does not enhance the solar cell's performance and may even slightly decrease it due to increased recombination and resistive losses.

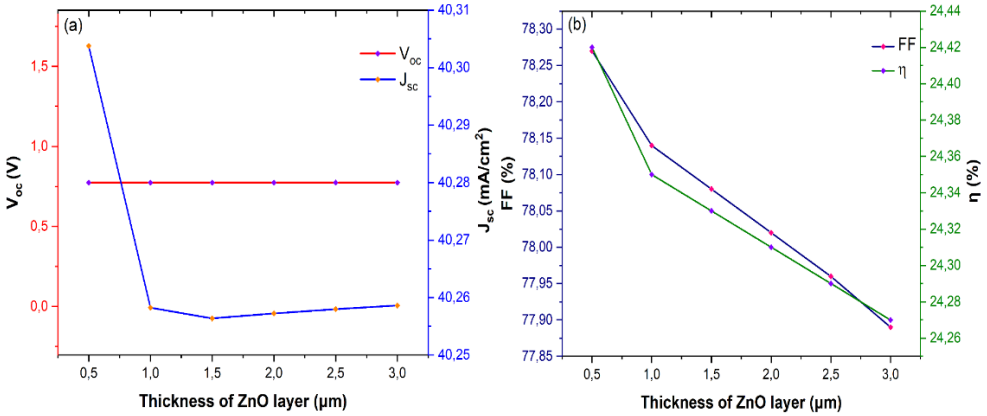

Fig. 5. Effect of thickness of ZnO layer on the performance parameters of the ZnO/SWCNT solar cell.

3.5 Effect of series resistance

To maximize efficiency of solar cell, minimizing series resistance (R_s). The study adjusted the R_s resistance range from 0 to 30 Ohm·cm² to investigate its effects on the parameters J_{sc}, V_{oc}, FF, and η of a ZnO/SWCNT solar cell, as shown in Fig. 6. Efficiency values of 24.42 % and 4.84 % were achieved for R_s settings of 0 and 30 Ohm·cm², respectively. As R_s increases, it restricts the current flow through the ZnO/SWCNT cell in the absence of applied voltage, resulting in a decrease in J_{sc}. This reduction in J_{sc} can lead to lower voltage drops across the ZnO/SWCNT cell, thereby increasing Voc. Additionally, higher R_s values tend to decrease FF by affecting the cell's ability to maintain high voltage and current simultaneously. These findings indicate that increasing R_s negatively impacts the ZnO/SWCNT solar cell, as evidenced by the significant decrease in efficiency with higher R_s resistance.

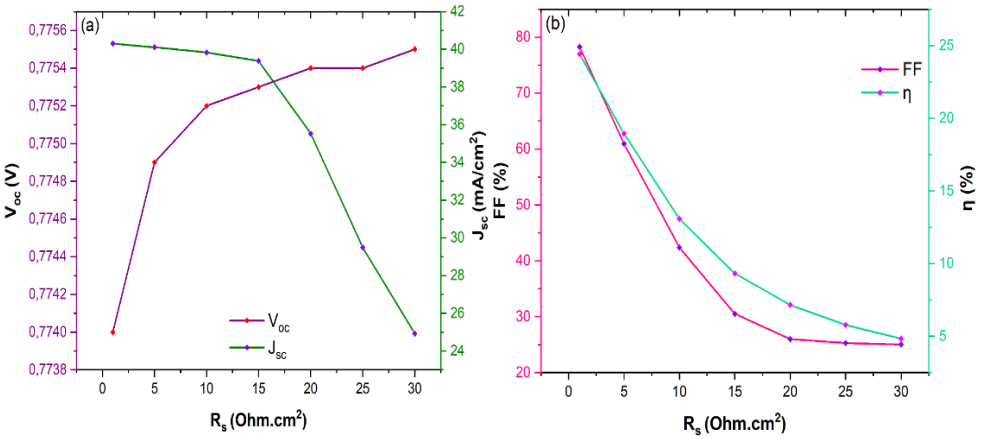

Fig. 6. Performance of simulated parameters in the ZnO/SWCNT solar cell as a function of R_s resistance.

3.6 Effect of shunt resistance

In this section, we examined the influence of shunt resistance (R_{sh}) on the performance of the ZnO/SWCNT solar cell. As illustrated in Fig. 7, it is clear that an increase in shunt resistance results in higher values for the parameters V_{oc}, J_{sc}, FF, and η. Specifically, efficiencies of 20.67 % and 24.42 % were achieved for R_{sh} values of 100 and 1000 Ohm.cm², respectively. Increasing R_{sh} reduces the leakage current through the solar cell, leading to lower charge recombination. This allows the cell to maintain higher V_{oc} voltages. Additionally, higher R_{sh} decreases parasitic current losses within the cell, thereby improving FF. Thus, by reducing recombination and parasitic current losses, an increase in R_{sh} enhances the efficiency of the ZnO/SWCNT solar cell. Furthermore, the change in J_{sc} despite the increased R_{sh} for the ZnO/SWCNT solar cell can be attributed to its effect on current photogeneration.

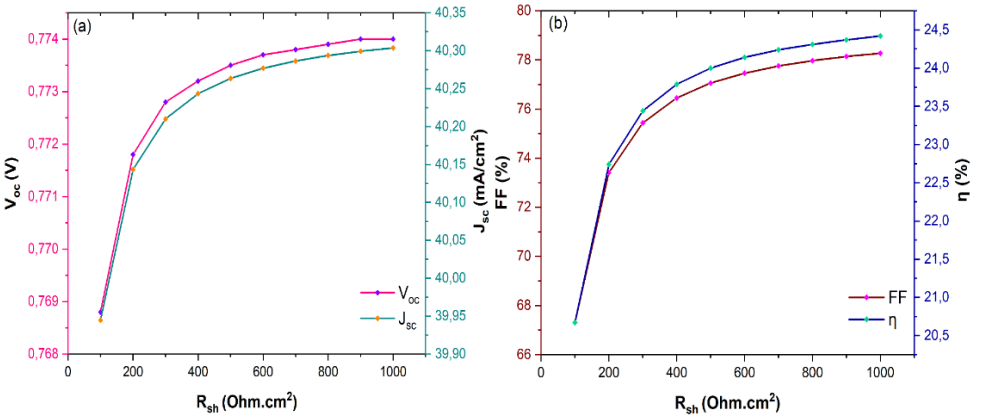

Fig. 7. Performance of simulated parameters in the ZnO/SWCNT solar cell as a function of R_{sh} resistance.

3.7 Optimized device

This study employed SCAPS-1D software to analyse the performance parameters of a ZnO/SWCNT solar cell. The findings reveal that increasing the thickness of the SWCNT layer significantly improves the device's overall efficiency. Conversely, increasing the thickness of the ZnO layer adversely affects the cell's performance. Furthermore, raising the operating temperature from 300K to 500K leads to a decline in the solar cell's efficiency. Additionally, optimizing the series resistance (R_s= 1 Ohm·cm²) and shunt resistance (R_{sh}= 1000 Ohm·cm²) enhances the cell's performance, as a higher R_{sh} and lower R_s positively influence its efficiency. Table 3 presents the optimized parameters for the ZnO/SWCNT solar cell, while Fig. 8 shows the J-V characteristics curve of this device after optimization. The redesigned solar cell exhibits a photovoltaic efficiency of 26.44%, a fill factor of 78.34%, a short-circuit current density of 43.35 mA/cm², and an open-circuit voltage of 0.7786 V. Table 4 provides a comparison of the photovoltaic parameters between the original and optimized devices.

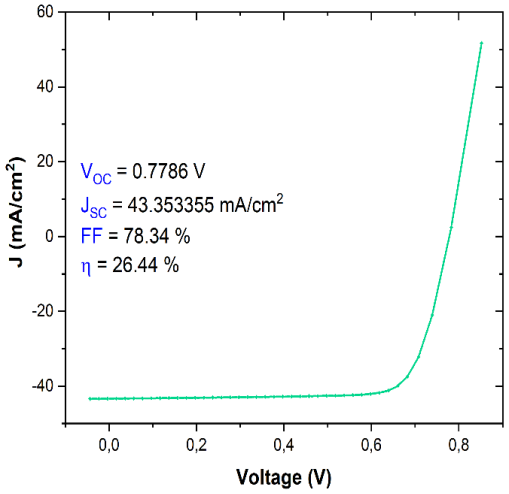

Fig. 8. J-V characteristics curve of the ZnO/SWCNT optimized device.

Table 3. The optimized parameters of the ZnO/SWCNT device.

Parameters	T(K)	d_{SWCNT}	d_{ZnO}	R_s	R_{sh}
Initial	300	0.15 µm	0.5 µm	1 Ohm.cm²	1000 Ohm.cm²
Optimized	300	3 µm	0.5 µm	1 Ohm.cm²	1000 Ohm.cm²

Table 4. Output parameters of the ZnO/SWCNT optimized device and those of the initial one.

Parameters	J_{sc}(mA/cm²)	V_{oc} (V)	FF (%)	η (%)
Initial	40.303777	0.7740	78.27	24.42
Optimized	43.353355	0.7786	78.34	26.44

3.8 Comparative study

A comparative analysis of experimental and theoretical studies on solar cells utilizing ZnO and SWCNT materials has been conducted. The remarkable electronic and optical properties of SWCNT highlight its potential as a promising component for integration into solar cell technologies, as illustrated in Table 5.

Table 5. Performance of solar cells incorporating ZnO and SWCNT materials.

Device	Parameters				Reference	Experiment/ Simulation
	J_{sc} (mA/cm^2)	V_{oc} (V)	FF (%)	η (%)		
ZnO/SWCNT	43.353355	0.7786	78.34	26.44	This work	Simulation
ZnO/GO	12.46	0.79	52.14	8.46	[26]	Simulation
ZnO/GO	7.24	0.72	56.94	9.12	[26]	Experiment
ZnO/PEIE	10.33	0.59	65	3.96	[27]	Experiment
ZnO-NR/SWCNT	7	0.69	56	2.7	[28]	Experiment
rGO/P3HT	49.713892	0.7717	75.67	29.03	[29]	Simulation

4 Conclusions

In this study, we used SCAPS-1D software to assess the performance of the ZnO/SWCNT solar cell. Our findings indicate that increasing the thickness of the SWCNT layer can enhance the overall performance of the device, whereas increasing the thickness of the ZnO layer may reduce it. The ZnO/SWCNT solar cell demonstrated an impressive power conversion efficiency of 26.44%, highlighting its potential as an effective photovoltaic light converter. Specifically, our SCAPS-1D simulations reveal a significant improvement in conversion efficiency due to the SWCNT layer. This underscores the potential of SWCNT as a valuable material for optoelectronic applications and light energy conversion.

Acknowledgement

Prof. Marc Burgelman, University of Ghent, Belgium, is heartily acknowledged by the authors, for providing the SCAPS-1D simulation software.

Conflicts of Interest

The authors declare that they have no conflict of interest.

References

1. M. Muzammil, K. N. Naam, M. Fareed, M. S. Hussain, M. Zulfiqar, Chemical Physics Impact **8**, 100407 (2024)
2. J. Arunachalam, K. Sivaperuman, Optik **303**, 171744 (2024)
3. T. Das, A. Guchhait, Materials Today: Proceedings, 26 January (2024). https://doi.org/10.1016/j.matpr.2024.01.039

4. A. Najim, O. Bajjou, M. Boulghallat, K. Rahmani, L. Moulaoui, E3S Web of Conferences **336**, 00006 (2022)
5. A. Najim, O. Bajjou, L. Moulaoui, A. Laassouli, M. Archi, A. Bakour, Y. Lachtioui, K. Rahmani, 3rd International conference on innovative research in applied science, engineering and technology (IRASET), 1–5 (2023)
6. A. Najim, O. Bajjou, A. Bakour, M. Boulghallat, K. Rahmani, Modern Physics Letters B **38**, 2450032 (2024)
7. A. Najim, O. Bajjou, M. Boulghallat, M. Khenfouch, K. Rahmani, Y. Chrafih, Optik **257**, 168874 (2022)
8. O. Bajjou, A. Najim, K. Rahmani, M. Khenfouch, J Mol Model **28**, 97 (2022)
9. A. Najim, O. Bajjou, A. Bakour, K. Rahmani, Journal of Electron Spectroscopy and Related Phenomena **265**, 147321 (2023)
10. L. Moulaoui, O. Bajjou, A. Najim, K. Rahmani, E3S Web of Conferences **336**, 00015 (2022)
11. L. Moulaoui, A. Najim, A. Laassouli, M. Archi, A. Bakour, Y. Lachtioui, K. Rahmani, O. Bajjou, B. Manaut, E3S Web of Conferences **469**, 00086 (2023)
12. A Laassouli, O Bajjou, Y Lachtioui, A. Najim, L. Moulaoui, K. Rahmani, 3rd International Conference on Innovative Research in Applied Science, Engineering and Technology (IRASET), (2023)
13. M. K. A. Mohammed, A. K. Al-Mousoi, S. Singh, A. Kumar, M. K. Hossain, S. Q. Salih, P. Sasikumar, R. Pandey, A. A. Yadav, Z. M. Yaseen, Optical Materials **138**, 113702 (2023)
14. S. Aseena, N. Abraham, V. S. Babu, Materials Today: Proceedings **43**, 3432–3437 (2021)
15. M. K. Hossain, G. F. I Toki, A. Kuddus, M. K. A. Mohammed, R. Pandey, J. Madan, S. Bhattarai, M. F. Rahman, D. K. Dwivedi, M. Amami, H. Bencherif, D. P. Samajdar, Materials Chemistry and Physics **308**, 128281 (2023)
16. L. Moulaoui, O. Bajjou, A. Najim, M. Archi, K. Rahmani, 2nd International Conference on Innovative Research in Applied Science, Engineering and Technology (IRASET), (2022)
17. S. Mushtaq, S. Tahir, A. Ashfaq, R. S. Bonilla, M. Haneef, R. Saeed, W. Ahmad, N. Amin, Solar Energy **249**, 401–413 (2023)
18. L. Moulaoui, O. Bajjou, A. Najim, K. Rahmani, A. Marouane, A. Laassouli, Y. Lachtioui, B. Manaut, 3rd International Conference on Innovative Research in Applied Science, Engineering and Technology (IRASET), (2023)
19. N. E. Ouarie, J. E. Hamdaoui, G. S. Sahoo, K. G. Rodriguez-Osorio, M. Courel, M. Zazoui, L. M. Pérez, D. Laroze, E. Feddi, Solar Energy **263**, 111929 (2023)
20. E. Danladi, A. C. Egbugha, R. C. Obasi, N. N. Tasie, C. U. Achem, I. S. Haruna, L. O. Ezeh, Journal of the Indian Chemical Society **100**, 101001 (2023)
21. L. Moulaoui, O. Bajjou, Y. Lachtioui, A. Najim, M. Archi, K. Rahmani, B. Manaut, J. Electron. Mater **52**, 7541–7553 (2023)
22. M. Q. Kareem, S. A. Hassan, S. S. Alimardan, S. M. Shareef, M. M. Ameen, Journal of Physics and Chemistry of Solids **188**, 111931 (2024)
23. A. Najim, O. Bajjou, A. Bakour, L. Moulaoui, K. Rahmani, Indian J Phys **98**, 67–77 (2024)

24. S. Sani, A. Usman, A. Bhatranand, Y. Jiraraksopakun, K. S. Muhammad, U. Yahaya, Materials Today Communications **38**, 107575 (2024)
25. H. Benali, B. Hartiti, F. Lmai, A. Batan, S. Fadili, P. Thevenin, Optik **304**, 171733 (2024)
26. S. Tyagi, P. K. Singh, A. K. Tiwari, Energy for Sustainable Development **70**, 205–224 (2022)
27. P. Li, L. Cai, G. Wang, D. C. Zhou, J. Xiang, Y. J. Zhang, B. F. Ding, K. Alameh, Q. L. Song, Synthetic Metals **203**, 243–248 (2015)
28. B. A. Albiss, M. I. Al-Widyan, I. Obaidat, Ceramics International **42**, 3563-3568 (2016)
29. A. Najim, L. Moulaoui, A. Bakour, O. Bajjou, K. Rahmani, J Opt (2024)